The Spatial Pattern of Response Magnitude and Selectivity for Orientation and Direction in Cat Visual Cortex

Nicholas V. Swindale, Amiram Grinvald[1] and Amir Shmuel[1,2]

Department of Ophthalmology and Visual Sciences, University of British Columbia, Vancouver, Canada V5Z 3N9, [1]Department of Neurobiology, The Weizmann Institute of Science, Rehovot, 76100, Israel and [2]Center for Magnetic Resonance Research, University of Minnesota, 2021 6th St. SE, Minneapolis, MN 55455, USA

Optical imaging studies of orientation and direction preference in visual cortex have typically used vector averaging to obtain angle and magnitude maps. This method has shown half-rotation orientation singularities (pinwheels) located within regions of low orientation vector magnitude. Direction preference is generally orthogonal to orientation preference, but often deviates from this, particularly in regions of low direction vector magnitude. Linear regions of rapid change in direction preference terminate in or near orientation singularities. The vector-averaging method is problematic however because it does not clearly disambiguate spatial variation in orientation tuning width from variation in height. It may also wrongly estimate preferred direction in regions where preference is weak. In this paper we analyze optical maps of cat visual cortex by fitting model tuning functions to the responses. This new method reveals features not previously evident. Orientation tuning height and width vary independently across the map: tuning height is always low near singularities, however regions of broad and narrow orientation tuning width can be found in regions of low tuning height, often alternating in a spoke-like fashion around singularities. Orientation and direction preference angles are always closely orthogonal. Reversals in direction preference form lines that originate precisely in orientation singularities.

Introduction

Optical imaging studies of orientation and direction preference in visual cortex have typically used vector averaging of responses as a function of stimulus orientation or direction to obtain angle and magnitude maps (Bonhoeffer and Grinvald, 1996). Such studies have shown that the orientation map is characterized by the presence of half-rotation singularities (or pinwheels) which are surrounded by regions in which vector magnitude is low. Direction preference is typically orthogonal to orientation preference, with lines of reversal in preference beginning and ending in, or near, the orientation singularities (Malonek *et al.*, 1994; Shmuel and Grinvald, 1996; Weliky *et al.*, 1996). Orientation and direction angles are often non-orthogonal however, particularly in regions of low vector magnitude, near the reversal lines and the singularities.

While vector averaging is a simple and fast way of computing maps of orientation and direction angle from single-condition images, it has drawbacks. Direction tuning curves obtained by optical imaging are, as in single-unit data, bimodal, with two peaks with variable relative heights, positions and widths. If the two peaks are of nearly equal height, or not 180° apart, the vector resultant angle may bear little relation to the position of the higher peak, and will not accurately reflect the direction of motion to which that region of cortex was most responsive (Kim *et al.*, 1999; Kisvardáy *et al.*, 2001). In addition, no information about the relative positions and heights of the two peaks in the direction tuning curve can be obtained, although these parameters are of interest. Vector averaging is probably an accurate way of estimating preferred orientation when applied to orientation tuning data (Swindale, 1998). However the interpretation of vector magnitude is problematic, since a low magnitude may be caused by either a low overall responsiveness of the point in question, or broad orientation tuning width. Although it has been suggested that variations in vector magnitude following division by the cocktail blank should reflect only variations in tuning width (Bonhoeffer *et al.*, 1995), in practice low vector magnitude has generally been regarded as indicative of either low responsiveness or broad tuning, or a combination of both [e.g. Bonhoeffer and Grinvald (Bonhoeffer and Grinvald, 1991)].

In this paper we have studied orientation and direction angle, tuning width and tuning height maps with an analysis method that avoids the limitations of vector averaging. It works by finding, at each location in the image, best-fitting model functions of the orientation or direction tuning responses. For orientation, the model is a circular normal (von Mises) function with parameters describing the position, height and width of the peak. For direction, the model is the sum of two such functions, which are unconstrained in their relative heights, widths and positions. We apply the method to optical data from area 18 of the cat and show that it reveals features not evident with vector averaging. Orientation and direction preference angles are always closely orthogonal and reversals in direction preference form lines that originate precisely in orientation singularities. Orientation tuning height is low in blob-shaped regions surrounding singularities. Bands of broad and narrow orientation tuning width, and of low and high direction selectivity, alternate in a spoke-like fashion around each singularity.

Materials and Methods

Data Acquisition

Single-condition images were obtained from area 18 of four anesthetized, paralyzed cats, using standard methods in experiments reported elsewhere (Shmuel and Grinvald, 1996, 2000). The stimuli were moving high-contrast square-wave gratings with a spatial frequency of 0.15–0.18 c/deg, and a temporal frequency of 2.5–6.0 Hz, presented binocularly. Sixteen directions of motion were used, spanning a 360° range at intervals of 22.5°. For three of the datasets (referred to as datasets 1–3), a limited amount of post-processing of the images was performed. Specifically, the images obtained during stimulation periods were divided by the images obtained during control periods in which an equi-luminant gray screen was presented. To remove slow noise of biological origin, a first frame analysis (Bonhoeffer and Grinvald, 1996) was performed: the first frame of the resulting division (corresponding to data obtained during the 0.5 s period prior to the stimulus and prior to the acquisition of the control) was subtracted from all subsequent frames. Division by the cocktail blank was avoided, as this would normalize the tuning curves and remove information about tuning height. It was noted that the mean pixel value of each of the 16 single-condition images was different, and these differences were not systematically related to stimulus orientation or direction. This apparently random variability in image means could be caused by slow spatial and temporal variations of blood volume during the

period of data acquisition. To remove this source of variability, image means were equalized by subtraction. Note that high-pass filtering would have done this in any case, since this removes the DC component of each image, in addition to other low frequencies. An additional justification for the procedure is that the overall goodness-of-fit values were substantially improved by it. The single-condition images were then smoothed by convolution with a Gaussian kernel with width = 50 μm. No other type of filtering was done. A fourth dataset (referred to as dataset 4) consisted of single-condition images pre-processed as described in Shmuel and Grinvald (Shmuel and Grinvald, 1996). This included division by the cocktail blank followed by high-pass and low-pass filtering.

Data Analysis

For each pixel in the image, the data to be analyzed consist of an optical response, measured at position (i, j) to one of N directions of motion, n = 1 ... N. For the present data there were 16 such values for each pixel. For each of these tuning curves we defined a baseline value, $b_{i,j}$, as the minimum of the response values for the pixel in question. We show below that this baseline, or stimulus non-specific response level, varies across the map, and has a structure that includes a spatially smooth, slowly varying component, as well as blood vessel artifacts, which are thereby removed from the analysis. Orientation and direction tuning parameters are thus defined in terms of the response evoked above this non-stimulus-specific background. Models in which the baseline was an independently variable parameter, fit to the tuning curves [as in Sharon and Grinvald (Sharon and Grinvald, 2002)] did not work well when tuning curves were broad (as was often the case with the present data) because tuning height and baseline values were insufficiently constrained by the data values and could be very variable.

To standardize the goodness-of-fit values, tuning curves were rescaled as follows: taking $H(i, j)$ as the difference between the maximum and minimum values of the responses at position (i, j) in the map, we define $H_{\max}$ as the largest value of $H(i, j)$ taken across the whole map. Tuning curves were rescaled by setting

$$R'_{i,j}(\varphi_n) = 100 \times (R_{i,j}(\varphi_n) - b_{i,j})/H_{\max} \quad (1)$$

Following this, every tuning curve in the map has a minimum value of zero, their shapes relative to each other remain unchanged, and all the data points comprising the tuning curves in the map lie between 0 and 100. Goodness-of-fit values can be interpreted as distances on this scale and compared between maps.

Analysis of Direction Tuning

Figure 1 (right panel) shows examples of optical direction tuning curves scaled as described in the preceding section. They are bimodal with peaks of varying relative height and width. Since orientation tuning curves are well described by a single circular normal (von Mises) function (Swindale, 1998) we decided to model these bimodal tuning curves as the sum of two circular normal functions, whose positions, heights and widths are unconstrained. The model function was

$$M(\varphi) = A_1\exp\{k_1(\cos(\varphi - \varphi_1) - 1)\} + A_2\exp\{k_2(\cos(\varphi - \varphi_1) - 1)\} \quad (2)$$

Here, M is the response, φ is the direction of stimulus motion, A_1 and A_2 are the heights of the individual peaks, φ_1 and φ_2 are the center directions of each peak and k_1 and k_2 are inversely related to the widths of each peak. Parameters A_1, A_2, φ_1, φ_2, k_1 and k_2 were adjusted to minimize the sum-of-squares error (or goodness of fit) defined by

$$f^2 = \frac{1}{N}\sum_{n=1}^{N}\left(R'(\varphi_n) - M(\varphi_n, A_1, A_2, \varphi_1, \varphi_2, k_1, k_2)\right)^2 \quad (3)$$

Preferred direction was defined as the center angle of whichever peak was higher, i.e. it was defined as φ_1 if $A_1 > A_2$, or as φ_2 if $A_2 > A_1$. Direction selectivity, D, was defined as

$$D = \mathrm{abs}\left(\frac{A_1 - A_2}{A_1 + A_2}\right) \quad (4)$$

This has a value of zero if the two peaks are equal in height, and has a maximum value of 1 if only one peak is present in the response.

Analysis of Orientation Tuning

Stimulus orientation was defined as the angle θ, at right angles to the direction of motion, mod(180), i.e.

$$\theta = \left|\varphi + 90^\circ\right|_{180} \quad (5)$$

Pairs of responses obtained to stimulus conditions 180° apart were averaged to obtain a single response at each of eight different stimulus orientations. The following model function was then fit to the data points:

$$O(\theta) = B\exp\left\{k\left[\cos 2\left(\theta - \theta_p\right) - 1\right]\right\} \quad (6)$$

where O is the model response, θ is the stimulus orientation, B is the maximum height of the orientation tuning curve, k is its width and θ_p is the preferred orientation. The half-width of the tuning curve at half-height, $\theta_{0.5}$ was calculated from k as

$$\theta_{0.5} = 0.5\cos^{-1}\left[\frac{(\ln 0.5 + k)}{k}\right] \quad (7)$$

This is subject to the condition that $k > -0.5\ \ln 0.5$. The value of k is still meaningful if it is less than this, but it means that the tuning function is so broad that it never has a value less than half its maximum height.

Least-squares Fitting

The Levenburg–Marquardt method (Press *et al.*, 1994) was used to fit the model functions to the data. Initial estimates of parameters were made as follows: for direction tuning data, A_1 = the maximum value of the data, $A_2 = 0.8A_1$, $k_1 = k_2 = 2.0$ ($\varphi_{0.5} = 50°$), φ_1 was set equal to the angle for which response was maximum and $\varphi_2 = \varphi_1 + 180°$; for orientation data the estimates were made similarly, with $k = 0.59$ ($\theta_{0.5} = 50°$). During the fits, the value(s) of k were constrained to be >0.1. This corresponds to a tuning curve that is almost flat. A fit was considered to have converged if the change in the goodness of fit, $\Delta f < 10^{-5}$ for 10 successive iterations of the fitting algorithm. After the fits, checks were made to ensure that parameter values lay within acceptable bounds. The fit was rejected if any of the following applied: (i) convergence had not occurred after 500 iterations; (ii) if the goodness of fit, $f > 10.0$; (iii) if B (or A_1 or A_2) < 0; (iv) if $\theta_{0.5} < 15°$ or $\varphi_{0.5} < 15°$. When parameters fell outside these bounds, it was clear from inspection that the tuning curve data were either noisy or flat with ill-defined peaks. These points tended to occur near the edges of the maps. They were excluded from subsequent data analyses by compiling separate masking images for the orientation and direction tuning analysis data.

Analysis programs were written in Compaq Visual Fortran™ and run under Windows 2000 on a 600 MHz Athlon PC. On average, it took ~1.2 ms to fit a directional tuning function to a set of 16 data points, and ~20–30 s to do a complete set of fits for an individual map.

Results

Goodness of Fit

Figure 1 shows examples of fits to orientation and direction data taken from randomly selected sites in one map. Other examples can be found in Figure 9. Table 1 gives averaged values of the goodness-of-fit measure, f, for individual maps. The means of these values for the four datasets studied were f = 2.9 for orientation and f = 3.5 for direction. Since pixel values were scaled to lie between 0 and 100, these values can be interpreted as distances on the same scale.

Table 1 also gives, for comparison, the values of f obtained when an angle-doubled cosine function (i.e. periodic over a 180° range) was fit to the orientation data, and when a cosine function (periodic over a 360º range) was fit to the direction data. The parameters adjusted in the fits were the absolute height, amplitude and phases of the cosines. As shown elsewhere (Swindale, 1998) vector averaging is mathematically equivalent to using a cosine as a model tuning function. Thus the phase angle returned by vector averaging will be identical to that returned by a cosine fit. (This was confirmed numerically.)

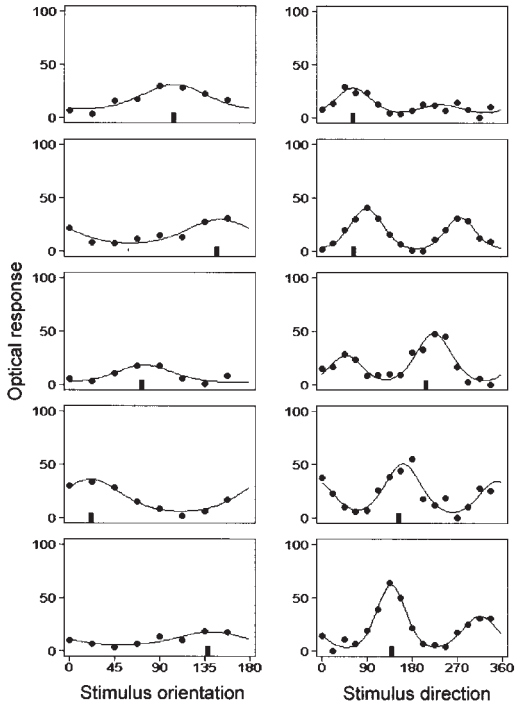

Figure 1. Examples of data and fitted model orientation (left panel) and direction (right panel) tuning curves. The black rectangle on the *x*-axis shows the corresponding vector estimate of orientation or direction. Note that for the direction data these estimates can be different from the position of the maximum response. Each graph is the tuning data from a single randomly selected pixel from dataset 1.

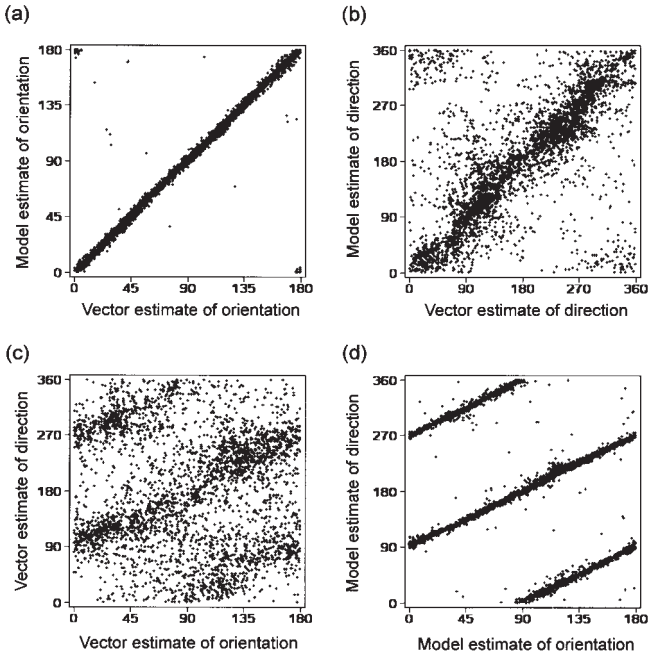

Figure 2. Scatter-plots showing the relationships between vector and model estimates of orientation and direction angle; each dot is a single map pixel: (*a*) relationship between vector and model estimates of orientation; (*b*) relationship between vector and model estimates of direction; (*c*) relationship between vector estimate of orientation and vector estimate of direction; and (*d*) relationship between model estimate of orientation and direction. Points come from dataset 3. For clarity, only odd-numbered pixels are shown, i.e. one-quarter of the pixels in the map.

Table 1
Goodness-of-fit values for model and vector methods

Dataset	Model orientation	Model direction	Cosine (vector) orientation	Cosine (vector) direction
1	3.20	3.92	4.23	11.98
2	3.61	4.10	3.99	8.65
3	2.44	2.99	2.95	7.90
4	2.47	2.90	3.39	11.1

Table 2
Difference between model and vector estimates of angle

Set	Orientation	Direction
1	–0.0 ± 6.3°	–1.1 ± 48.7°
2	–0.2 ± 8.6°	–0.12 ± 51.8°
3	–0.1 ± 5.0°	0.32 ± 51.9°
4	–0.1 ± 4.5°	6.0 ± 50.0°

Table 1 shows that the cosine provided a slightly worse fit than the model function for orientation tuning data, for all four datasets (the average of f across all four maps was 3.6). Similarly, the cosine provided a much worse fit (f = 9.9) for the directional tuning data. This value was in fact only slightly better than that obtained by fitting a horizontal line to the data, for which the average value of f = 10.9.

Comparison with Estimates Obtained by Vector Averaging

The estimates of orientation and direction obtained with the model fits were compared with those obtained by vector averaging (Fig. 2*a*,*b*). There is good agreement between the estimates for orientation, but not for direction. Table 2 shows, for each of the four datasets analyzed, the means and standard deviations of the difference between the model and vector estimates of orientation and direction angle. In all cases the mean difference is close to zero, which is not surprising given the lack of any expected systematic difference between the two types of estimate (e.g. a clockwise orientation difference). The standard deviations of the differences show by how much the estimates tend to differ. For orientation, the differences are small, with estimates generally being within about ±6° of each other. For direction, the differences average about ±51°, indicating substantial disagreement between the methods. One reason for considering the model-fitting estimate to be the better of the two is that it corresponds more accurately to the angle of stimulus motion that gives the largest cortical response. Reasons for these large differences are considered further in the Discussion.

Relationship Between Orientation and Direction Preference Angles

As in previous studies (Malonek *et al.*, 1994; Shmuel and Grinvald, 1996; Weliky *et al.*, 1996), we found that the vector estimates of orientation and direction were often non-orthogonal (Fig. 2*c*). The model estimates, however, were much closer to orthogonal (Fig. 2*d*). Table 3 shows the means and standard deviations of the differences between direction and orientation angles for the vector and model estimates. The mean differences are close to 90° for both methods, which is expected given the lack of any systematic clockwise or anticlockwise bias, but the

Table 3
Difference between direction and orientation angles

Dataset	Vector averaging	Model fits
1	89.6 ± 39.6°	90.3 ± 9.2°
2	91.7 ± 42.4°	90.4 ± 11.3°
3	92.6 ± 39.6°	90.5 ± 7.0°
4	85.0 ± 43.1°	89.4 ± 8.3°

Table 4
Difference between the two peaks in the direction tuning curves

Dataset	Mean ± SD
1	180.6 ± 20.8°
2	180.9 ± 23.2°
3	181.1 ± 16.0°
4	178.7 ± 16.8°

standard deviations for the model fits (~±9°) are substantially less than those obtained with vector averaging (~±41°).

The finding that orientation and direction preference angles are always nearly orthogonal can be attributed to the empirical observation that the two peaks in the direction tuning curves are always close to 180° apart (Table 4). This means that the angle given by the higher of the two peaks will generally be close to the angle given by curve fitting when the two peaks are averaged [i.e. angles on the *x*-axis taken modulo(180) rather than modulo(360)]. This agreement will persist, even when the two peaks are of similar height. In this case, however, the vector method often returns angles that are different from the position of either peak. Figure 3*a* shows that the difference between the model and vector estimates of direction angle is largest for points with low values of direction selectivity.

Spatial Layout of Orientation Tuning Parameters

Figures 4 and 5 show maps obtained from model fits of orienta-

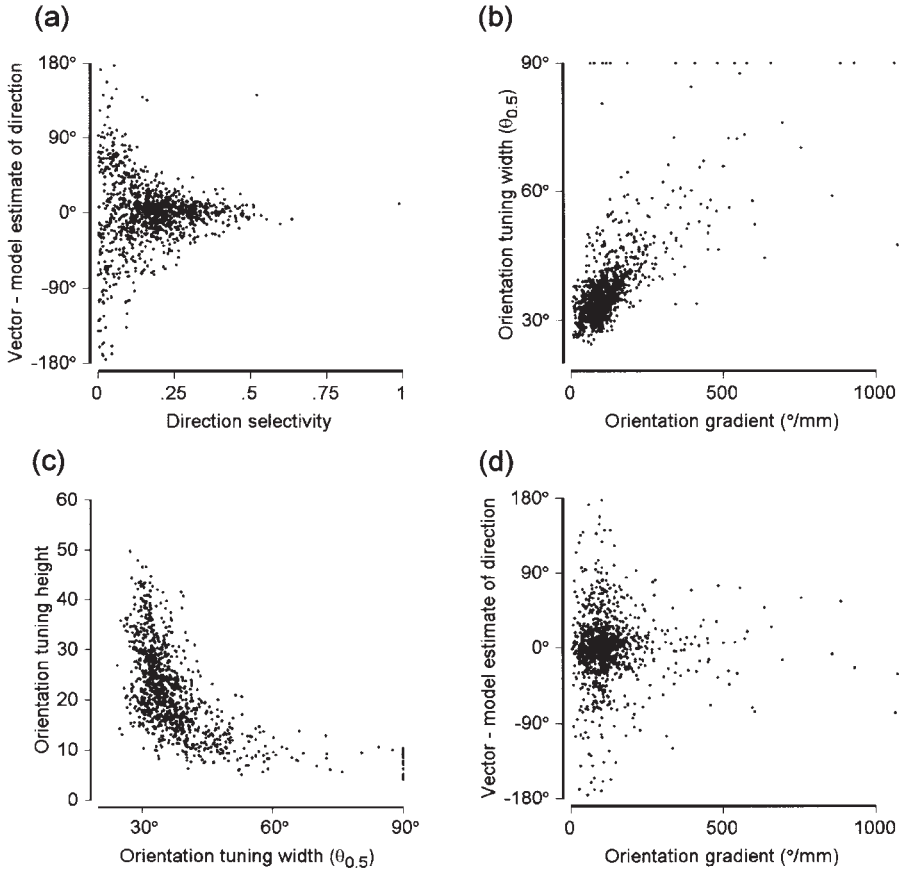

Figure 3. (*a–c*) Relationships between selected map parameters. Each graph shows data from 1000 points taken at random (avoiding duplication) from dataset 1. Results from other maps were qualitatively similar except for (*c*) where in datasets 2 and 3 fewer points with orientation tuning height values greater than 30 were present

Figure 4. (top) Maps of parameters obtained by the model-fitting method. Singularity positions and signs are indicated by green (positive) and red (negative) asterisks or circles. (*a*) Orientation angle; (*b*) direction angle, with white pixels indicating direction fractures; (*c*) orientation tuning width (half-width at half-height); (*d*) direction selectivity (*D*, equation 7; low (dark) pixels mean low selectivity); (*e*) orientation tuning height (low height = dark); (*f*) relationship between fractures (black lines) in the direction map and positive and negative orientation singularities. All maps are from dataset 1 and are at the same scale. Grey pixels in (*a*) and (*b*) are those masked out because of unacceptable fits; the same points are shown in dark red in (*c*)–(*e*). Scale bar in (*a*) = 1 mm. Arrows indicate medial (M) and posterior (P) on the cortex.

Figure 5. (bottom) Maps of parameters obtained by the model-fitting method in dataset 3. Layout of panels and interpretation of grayscale values is the same as in Figure 4. Scale bar in (*a*) = 1 mm. Arrows indicate anterior (A) and medial (M) directions.

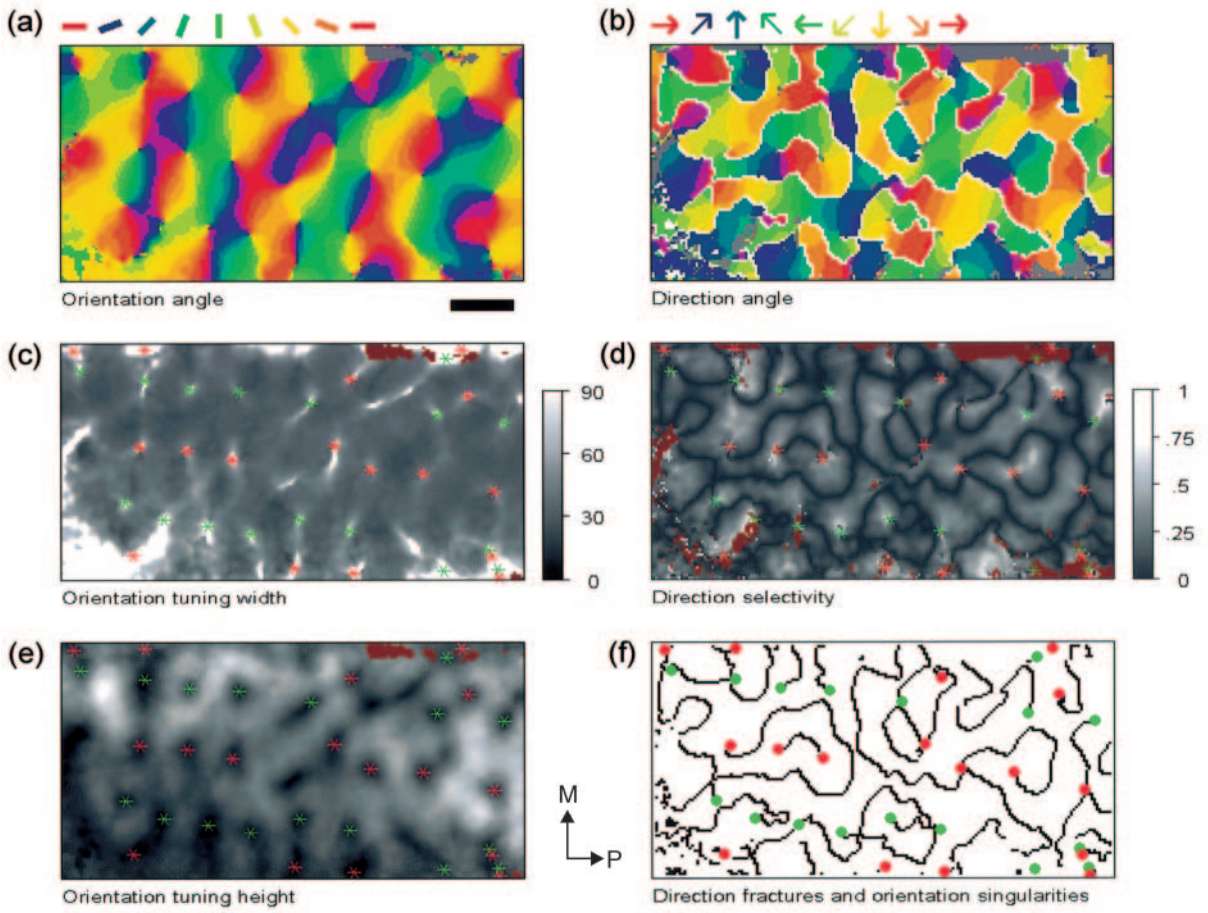

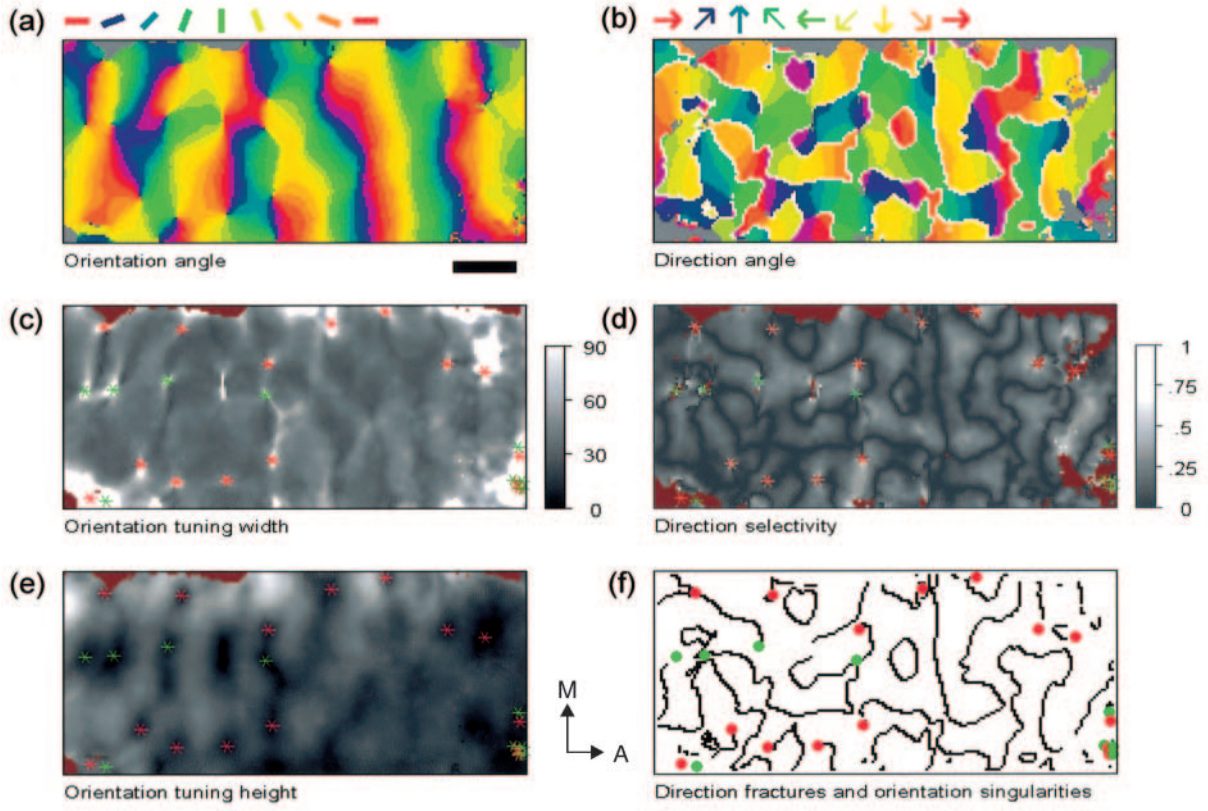

tion angle (Figs 4*a* and 5*a*), orientation tuning width (Figs 4*c* and 5*c*) and orientation tuning height (Figs 4*e* and 5*e*). Positive and negative singularities in the orientation map are shown in Figures 4 and 5 as green (= positive) or red (= negative) asterisks or circles. Positive singularities are defined as those for which orientation values rotate in a clockwise direction as a clockwise circuit is made around the singularity; negative singularities are those where orientations rotate in an anticlockwise direction for a clockwise circuit. The tuning height maps (Figs 4*e* and 5*e*) resembled maps of vector magnitude, and contained circular or elongated regions of low tuning height ~200–400 μm in diameter. An orientation singularity was present in many, although not all, of such regions. Singularities were never found outside regions of low tuning height.

One-dimensional profiles through the tuning height, width and baseline maps were examined. Profiles passing through singularities showed periodic increases and decreases in tuning height and width, superimposed on an irregularly fluctuating baseline level (Fig. 6). (The behavior of the baseline is considered in more detail below.) We calculated how, on average, tuning curve height and width varied as a function of radial distance from a singularity. For this analysis, only singularities that were more than 250 μm distant from any other singularity were included, and the single-condition images from which the tuning maps were derived were either not smoothed (datasets 1 and 3) or minimally smoothed with a Gaussian of width σ = 25 μm (dataset 2). Figure 7*a–c* shows the resulting functions, which are similar for all three datasets. Average tuning width decreases rapidly with distance from singularities, reaching a minimum at 425 μm (dataset 1) or 350 μm (datasets 2 and 3). It then rises, and at a distance of ~750 μm is similar to the average value taken over the whole map. A similar, but inverted, pattern of variation occurs in tuning height. However a closer comparison of the functions, following inversion and scaling of the tuning height function to match that of tuning width (Fig. 7*d–f*), shows that the pattern of variation is not exactly the same: tuning width falls off somewhat more rapidly than tuning height rises. On average, tuning width falls to near baseline values at a distance of 175 μm (dataset 1) or 150 μm (datasets 2 and 3); tuning height on the other hand rises to baseline values at distances of 225 μm (dataset 1) and 200 μm (datasets 2 and 3).

The preceding analysis ignores the fact that the pattern of variation of tuning width around singularities is often not radially symmetric (Figs 4*c*, 5*c*, 8 and 9). Typically, although not always, one or more regions of broad orientation tuning extend from each singularity in a short strip (Figs 8*b*,*c*,*e*, *f*). Tuning curve height remained low in these regions (Fig. 8, thin black lines). Regions of narrow tuning width could be found close (<100 μm) to singularities. Figure 9 shows examples of orientation tuning curves and variations in tuning width observed at points close to, and in, a singularity. Similar patterns of variation were seen in all four datasets.

There was a positive correlation between tuning width and orientation gradient across the whole map (Fig. 3*b*): tuning width was narrow in regions of low spatial rates of change of orientation preference and vice versa (r = 0.68, 0.62 and 0.63 for datasets 1, 2 and 3, respectively). There was a negative, L-shaped, correlation between tuning width and tuning height (Fig. 3*c*): points with broad tuning always had low tuning height, while highly responsive curves were always narrowly tuned. However the reverse was not always the case, and narrow tuning width could be associated with small as well as large tuning heights.

In theory, if orientation tuning curves of different widths and heights are normalized (by dividing by the sum of the responses, or the cocktail blank) the vector magnitude will depend only on the tuning width (Wörgötter and Eysel, 1987; Swindale, 1998). A previous analysis that looked at variation in orientation tuning curve width using this method (Bonhoeffer *et al.*, 1995) showed only a local isotropic broadening of selectivity close to orientation singularities, unlike the changes observed in the present study. We confirmed that this difference is due to our subtraction of baseline activity from the single-condition maps before analysis. If we did not do this subtraction, images of the normalized vector magnitude showed a spatial pattern of variation similar to that observed by Bonhoeffer *et al.* (Bonhoeffer *et al.*, 1995). If the baseline was subtracted before normalization, the images of vector magnitude looked similar to those seen in the tuning width maps obtained with the model fitting method. We confirmed by calculations with model tuning curves that adding a constant baseline response to orientation tuning curves of different heights and widths re-introduces a relationship between tuning height and vector magnitude following normalization.

Spatial Layout of Direction Tuning Parameters

Angle maps of direction preference (Figs 4*b* and 5*b*) show clearly defined iso-direction domains bounded in part by linear 'fractures' across which direction preference changes by 180°. Figure 9*b* shows that these lines are not discontinuities but represent points of equality in the heights of the two peaks in the direction tuning curve. As reported previously in cat areas 17 (Kim *et al.*, 1999) and 18 (Swindale *et al.*, 1987; Shmuel and Grinvald, 1996), owl monkey MT (Malonek *et al.*, 1994) and ferret area 17 (Weliky *et al.*, 1996), these reversal lines appear to begin and end close to singularities. However here the relationship is even more clear, with odd numbers of fracture lines terminating quite precisely at singularity locations.

The map of direction selectivity (Figs 4*d* and 5*d*) shows linear regions of low selectivity (dark regions in the figure) that coincide with the fractures, and abut singularities. Regions of

Figure 6. A one-dimensional transect through a portion of the map shown in Figure 4, showing the variation in orientation tuning height (●), tuning width (○) and the baseline signal (—). The transect passes through 3 singularities.

Figure 7. Graphs showing the variation in average orientation tuning height (●), orientation tuning width (○) and the baseline signal (—) as a function of distance in microns from singularity positions. Only points around singularities that were more than 250 μm distant from any other singularity were included in the analysis. (*a*) Dataset 1 (20 singularities); (*b*) dataset 2 (14 singularities), (*c*) dataset 3 (13 singularities). The *y*-axis on the left gives tuning width in degrees at half-height; the *y*-axis on the right gives tuning curve and baseline height in scaled units according to equation 1. A constant has been subtracted from the baseline values in each case for clarity. (*d*)–(*f*) show the height and width values for each of the three datasets rescaled so the values at the origin = 100 and average values between 1000 and 1500 μm = 0.

Figure 8. Patterns of variation of orientation tuning width (●) and height (—) around singularities. The left-hand axis shows tuning width in degrees at half height, and the right-hand axis shows tuning height in scaled units. The *x*-axis shows distance in degrees around the circumference of a circle (white dots) around each singularity. Examples (*a–c*) are from dataset 1 (circle radius = 0.25 mm), (*d–f*) are from dataset 2 (radius = 0.14 mm) and (*g–i*) are from dataset 3 (radius = 0.3 mm).

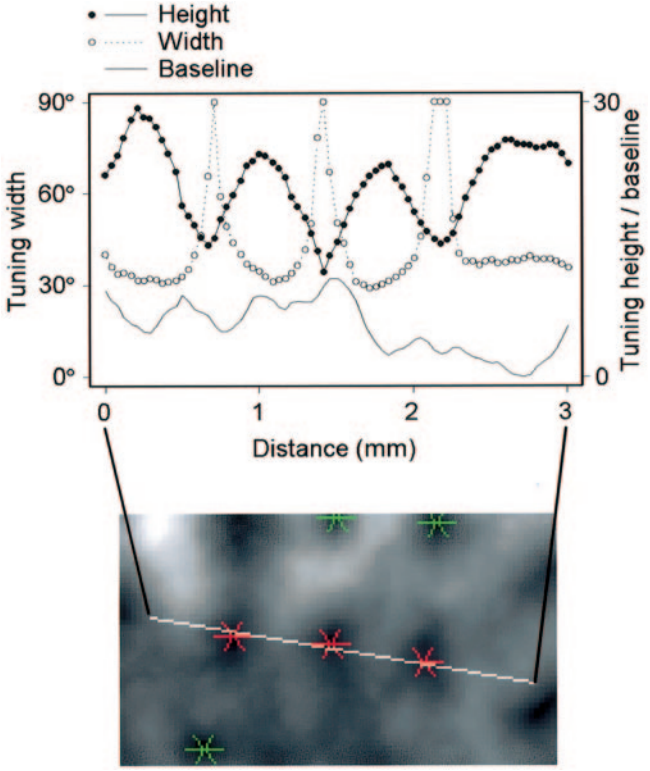

Figure 6

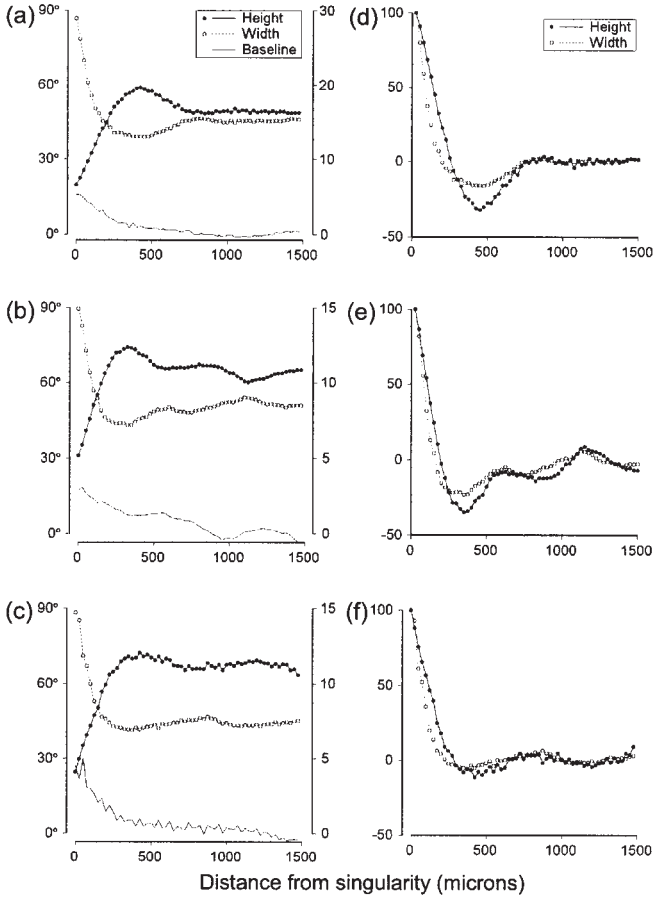

Figure 7

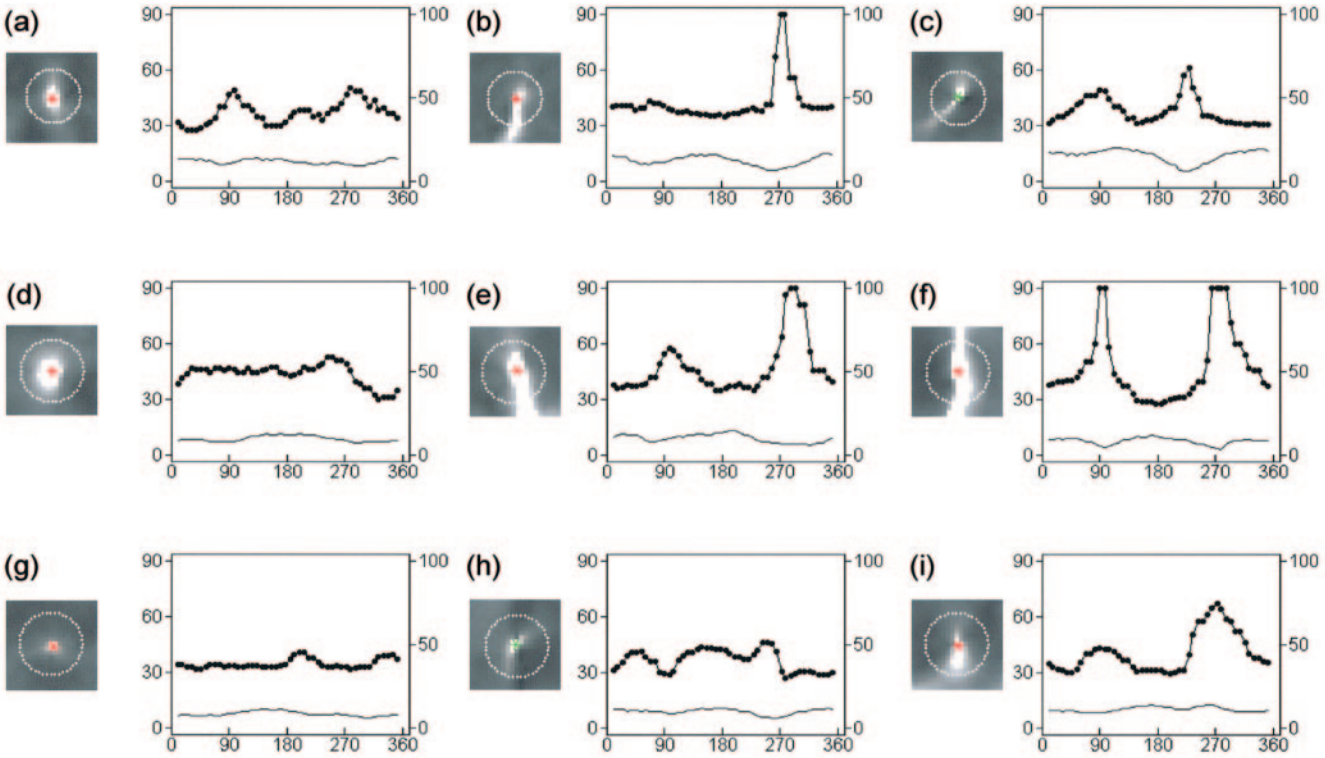

Figure 8

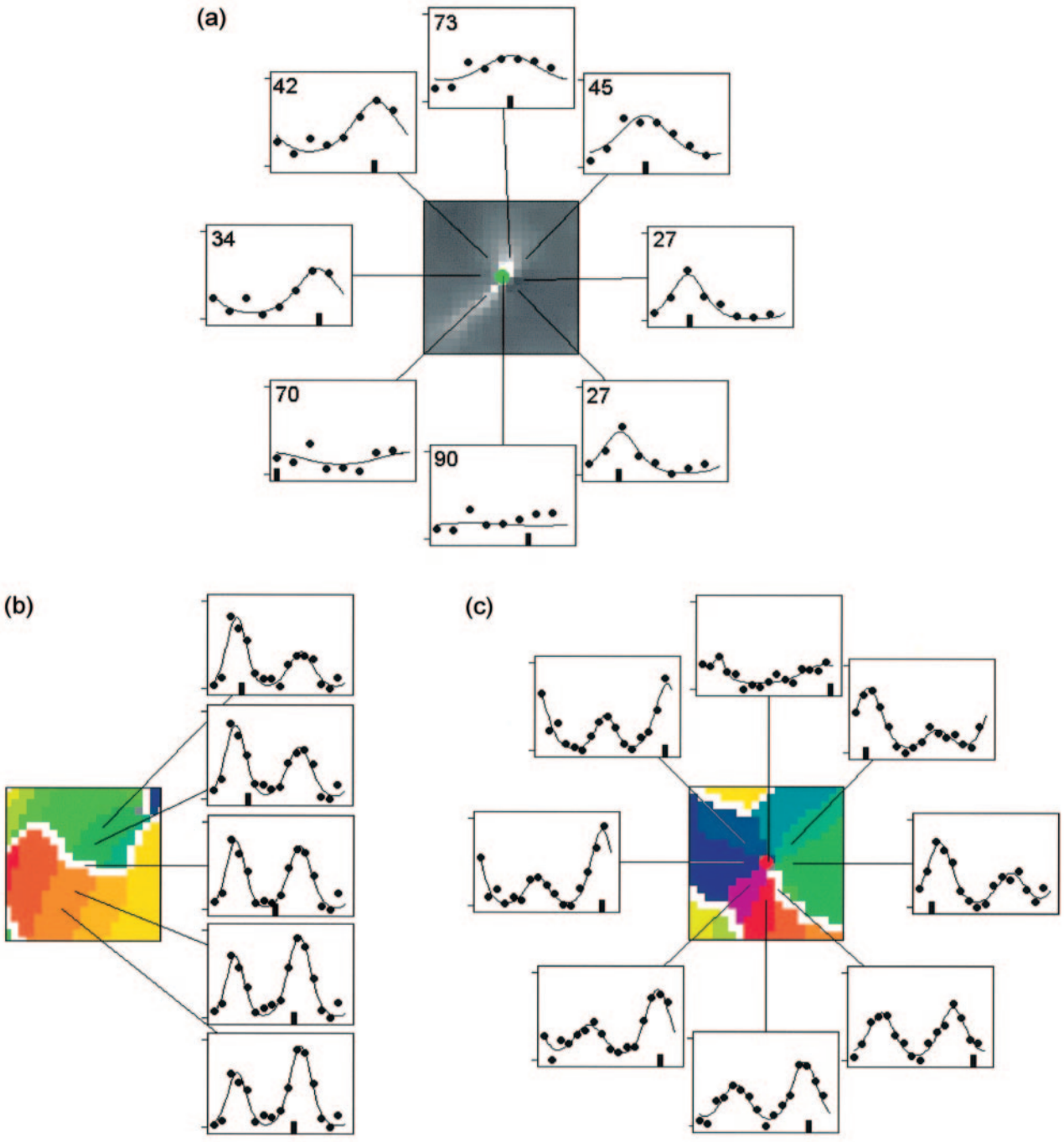

Figure 9. Tuning curves from specific map regions. Each region is 20 pixels, or 0.5 mm, wide. In all the graphs the vertical scaling (tick marks) is from 0 to 50, and the small black rectangle indicates the angle or direction obtained from the same data by vector averaging. (*a*) An orientation tuning width map (bright pixels = broad tuning) around a central singularity (green spot); the surrounding panels show orientation tuning data and the model fits from the indicated points. (The same singularity is shown in Fig. 8*c*.) Tuning widths (half-width at half-height in degrees) are shown for each tuning curve in the top left of each panel. Horizontal axes run from 0 to 180°. (*b*) Portion of a direction angle map showing direction fractures (white lines); right-hand panels show direction tuning curves from indicated points in the map. Horizontal axes run from 0 to 360°. Note that the relative height of the two peaks changes across the fracture; on the fracture itself the heights are nearly the same. (*c*) Variation in direction tuning around an orientation singularity (red spot) at the center of the panel where a direction fracture (white line) terminates.

high selectivity lie in between the fracture lines, and, surprisingly, can often be found close to singularities, opposite a region of low selectivity. An increase in direction selectivity with decreasing distance from a singularity implies that the height of the smaller of the two peaks decreases at a faster rate than the other peak as the singularity is approached. Figure 9*c* shows examples of direction tuning curves obtained close to a singularity.

Effects of Smoothing on Spatial Patterns of Tuning and Responsiveness

While the complex patterns of tuning and responsiveness within

the pinwheel regions are of interest, they do not necessarily reflect the properties of individual neurons in the same regions or even the mean activities of neurons in the imaged location. Light scattering, blurring caused by signals from out-of-focus layers, the spatially smooth (or blurred) nature of the hemodynamic signal, and smoothing done after the images have been acquired might affect the signals from regions where properties are changing relatively rapidly. We investigated this possibility in two ways. First, we examined data where no post-acquisition smoothing of any kind had been done. As expected, the angle, height and width maps were noisier, but the pattern of orientation tuning height and width, and of direction selectivity, around the singularities and elsewhere was similar to that observed with the smoothed data. As a second test we took the angle maps of orientation and direction preference resulting from the model fits, and then generated simulated single-condition images assuming a fixed tuning height, a fixed tuning half-width at half-height of 30° and a fixed direction selectivity, $D = 0.20$. We then smoothed the simulated single-condition maps with a Gaussian kernel with widths, σ, varying from 20 to 300 μm. New tuning width and selectivity maps were then calculated. For intermediate amounts of smoothing ($\sigma \sim 150$ μm) the control maps resembled the real ones in their general appearance (Fig. 10*a–d*). The similarity was further evaluated by

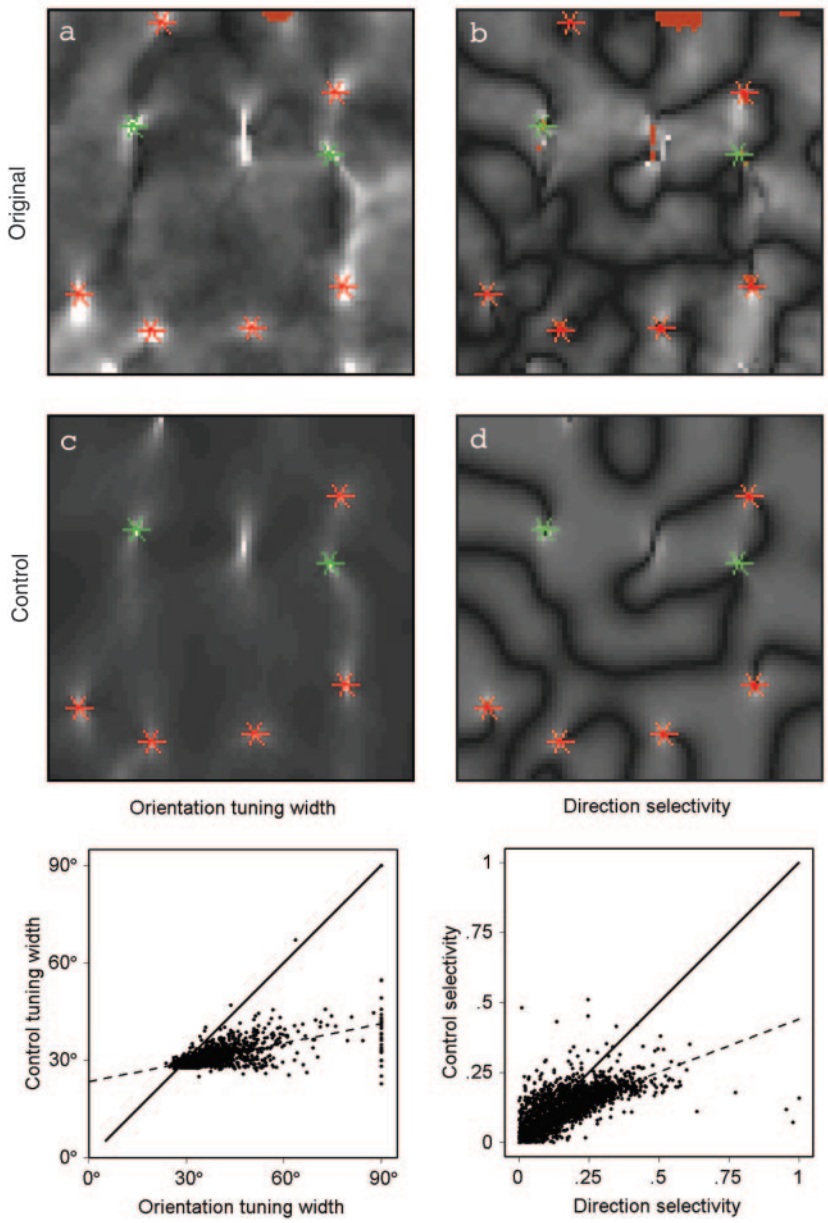

Figure 10. Control for the effect of optical blur on orientation tuning width and direction selectivity. (*a*) and (*b*) are the original width and selectivity maps; (*c*) and (*d*) are control images, obtained as described in the text after smoothing single-condition images with an isotropic Gaussian with a width $\sigma = 150$ μm. Images are from dataset 3. The relationship between the grayscale values and tuning values are the same for the control and normal cases; (*e*) and (*f*): the relationship between selectivity measures observed experimentally (*x*-axes) and values resulting from the Gaussian smoothing controls (*y*-axes) described in the text, with a smoothing radius $\sigma = 150$ μm. (*e*) is for orientation tuning width (degrees at half height) and (*f*) is for direction selectivity, *D* (equation 4). Dashed lines are fit by linear regression to the data points; the solid lines show $y = x$.

calculating, for each pair of control and real maps, and a particular smoothing width: (i) the correlation between the orientation tuning width values; (ii) the slope of the correlation, and (iii) the root mean square (r.m.s.) of the difference in the values. A similar analysis was done for direction selectivity. Table 5 shows the results for tuning width for dataset 1 for a variety of smoothing widths. (Values for datasets 2 and 3 show smaller correlations, smaller slopes and larger r.m.s. difference values.) While strong positive correlations between the measured and control tuning width values were found, the slopes of the correlations were substantially less than 1 across a range of smoothing width values (Fig. 10*e*,*f*). This was true for both orientation tuning width and direction selectivity values (Table 6), in all three of the datasets that were tested. Additional tests with a range of initial selectivity values and smoothing widths were done (data not shown), and these gave no indication that other combinations of parameters would give closer similarity between the real and control maps. These results suggest that the observed variations in orientation tuning and direction selectivity can be only partly explained (or modeled) as the result of isotropic Gaussian blurring of signals. The remaining variations may be real, perhaps caused by network interactions that are not locally isotropic or are non-Gaussian in character.

Table 5
Comparison of observed and control orientation tuning width values in dataset 1

Smoothing radius (μm)	r^2	Slope	r.m.s. difference
0	0	0	14.3
20	0.52	0.02	14.1
50	0.46	0.11	13.0
75	0.50	0.15	12.3
100	0.49	0.18	11.6
150	0.37	0.20	10.6
200	0.28	0.21	10.1
250	0.17	0.19	10.1
300	0.14	0.20	10.1

Table 6
Comparison of observed and control direction selectivity values in dataset 1

Smoothing radius (μm)	r^2	Slope	r.m.s. difference
0	0	0	0.12
20	0.25	0.08	0.11
50	0.41	0.29	0.10
75	0.50	0.36	0.09
100	0.52	0.39	0.09
150	0.46	0.39	0.10
200	0.31	0.34	0.12
250	0.19	0.27	0.13
300	0.11	0.21	0.14

The Baseline Response

A priori it seems likely that the baseline signal, *b* (i.e. the minimum response value at each pixel; see Materials and Methods) might be a mixture of blood vessel artifacts common to all images, spatial fluctuations in the hemodynamic signal unrelated to the stimuli, and real variations in stimulus-non-specific responses. These possibilities are consistent with the appearance of the baseline images (Figs 6 and 11) inasmuch as they contain low-spatial frequency variations, and bright streaks that coincide with the blood vessels observed in the mapped regions (images not shown). Further examination of the images suggested a weak tendency for some singularities to be located in regions where there was a small local elevation in the baseline. Overall correlations (i.e. taken over an entire map) between orientation tuning height and baseline (Table 7) were positive in two cases (datasets 1 and 3) and close to zero in the other (dataset 2). However these correlations represent trends averaged over the entire map, and an opposite trend might be present locally, in regions of low tuning height close to singularities. To test for that, we calculated the average of the baseline signal as a function of radial distance from a singularity, in the same way that we calculated the variation in tuning height and width. The resulting functions showed an increase in baseline with decreasing distance from singularities for all three non-normalized datasets (Fig. 7*a–c*). We observed that the baseline increase was often not clearly evident at individual singularities (e.g. Fig. 11) and that there were many regions (e.g. the right-hand side of Fig. 6) where pronounced height and width variations occurred that were not systematically related to the variation in baseline magnitude.

Table 7
Correlation between baseline activity and orientation tuning height

Dataset	r^2	Slope
1	0.10	0.30
2	0.003	0.02
3	0.35	0.42

Discussion

Comparison of the Model and Vector Methods

Vector averaging treats optical responses as vectors whose length is proportional to the response and whose angle relative to the origin is given by either twice the stimulus orientation, or by the direction of stimulus motion. In the latter case, the resultant angle gives the estimated direction preference, while for orientation the angle of the resultant is halved to find the estimated best orientation. Mathematically, these procedures are identical to performing a least-squares fit of a cosine function with variable phase and amplitude (Swindale, 1998). They are also identical to finding the phase angle of the first and second harmonic Fourier components of the data (Wörgötter and Eysel, 1987). It has been shown that a cosine provides a much less good description of single-unit orientation tuning data than does the circular normal function (Swindale, 1998). In the present study, the mean goodness of fit obtained with an angle-doubled cosine was only slightly worse than the value obtained by fitting the model function (Table 1). Accordingly, estimates of preferred orientation did not differ substantially between the two methods, although it is reasonable to expect that the model estimate should be the better of the two. In contrast, a cosine is *a priori* a bad description of directional tuning data, since a function with one peak is being fit to data in which two peaks are generally present. When a cosine was fit to the direction tuning data, the mean goodness of fit was substantially worse than the value obtained by fitting the model function and was only slightly better than the value obtained by fitting a horizontal line (the r.m.s. value of the points in each tuning curve about their mean). Vector averaging gives reasonably accurate estimates of the position of the higher of the two peaks when one is substantially higher than the other, however in regions of low direction selectivity the angles returned may bear little relation to the position of either peak [Figs 1, 3*a*, 9*b*, middle graph; see

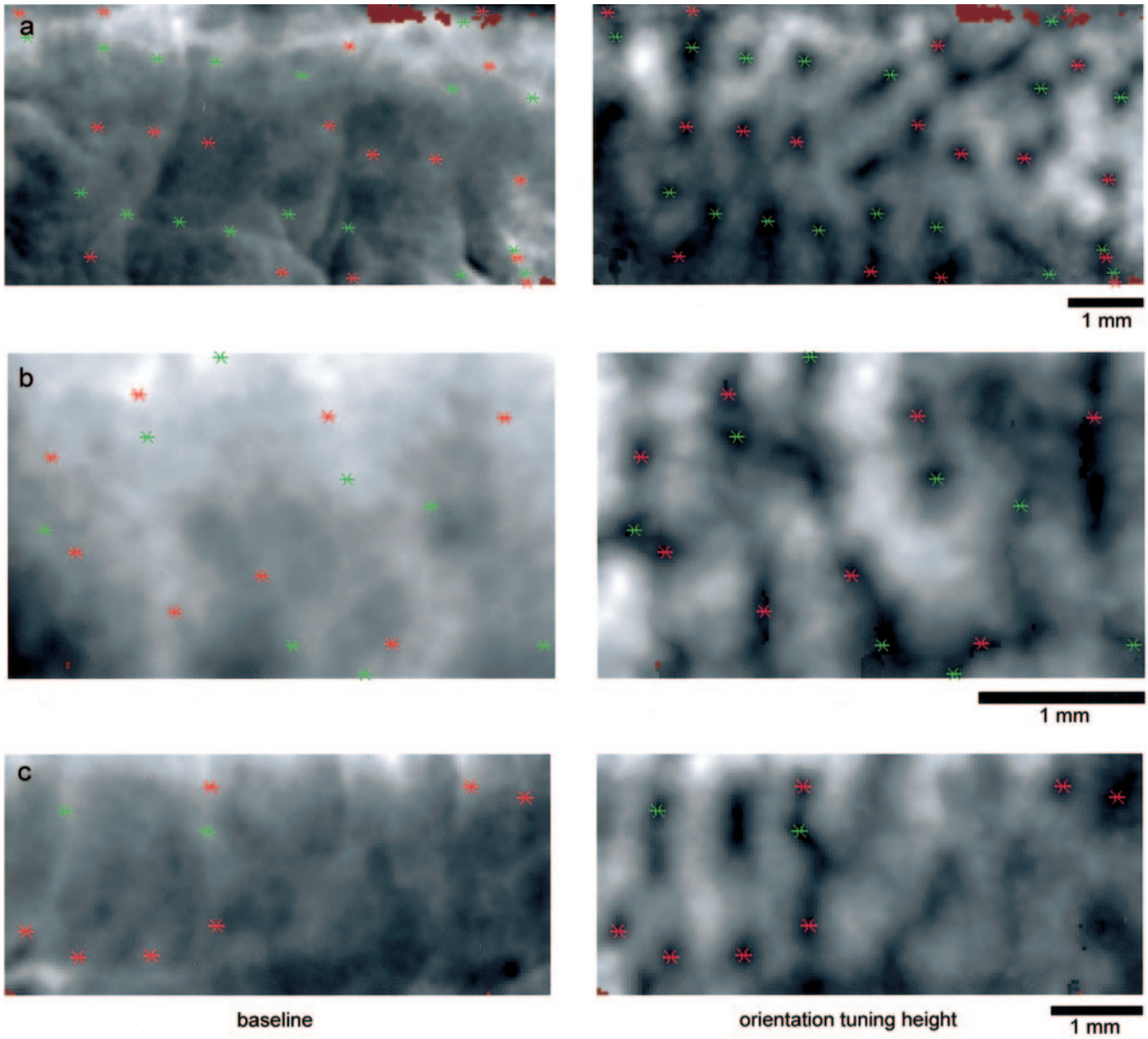

Figure 11. Images showing the variation in the baseline level, *b* (as defined in the Methods), across the map (left panels), together with the corresponding orientation tuning height maps (right panels). Brightness scaling is the same for both types of map: here, bright pixels correspond to an increase in optical response or an increase in tuning curve height. Singularity locations are indicated by asterisks (green = positive, red = negative). (*a*) Images from dataset 1, (*b*) images from dataset 2, (*c*) images from dataset 3.

also Fig. 10*a* in Shmuel and Grinvald (Shmuel and Grinvald, 1996), or Fig. 2*a* in Weliky *et al.* (Weliky *et al.*, 1996)]. Errors can occur even when the two peaks are dissimilar in height (e.g. Figure 1, second graph from top in right-hand column). With the model fitting method the direction preference angle is almost always closely orthogonal to the angle of orientation preference. As a result, iso-direction domains have sharply defined boundaries that intersect the direction fracture lines at well defined angles (Figs 4*b* and 5*b*).

Comparison of the Model Method with Previous Approaches

Other authors have pointed out the weakness of the vector method when applied to direction tuning data. Alternatives proposed involve interpolating between data points to estimate the maximum (Kim *et al.*, 1999) or simply taking the direction for which response is maximum (Kisvardáy *et al.*, 2001). We believe that our solution to the problem may have advantages over these methods. First, neither method yields parameter values that correspond to aspects of tuning curve shape other than the position of the peak. Secondly, simply taking the position of the maximum response (Kisvardáy *et al.*, 2001) ignores information in the rest of the tuning curve data that could be used to establish the position of the peak more precisely. For this reason, the method is likely to perform poorly when tested with noisy data. The interpolation method (Kim *et al.*, 1999) does not have this problem. It has the advantage over our method of not requiring iterative least-squares fitting, and is similar inasmuch as it involves an implied fit to the tuning curve data of a model function that is the sum of a series of sine and

cosine terms. A direct comparison of this method and ours would require comparing the goodness of fit of each model function to the data, the assumption being that the model giving the better fit gives the better estimation of direction preference. Neither of the previous methods addresses, as does ours, the issue of disambiguating variations in tuning height and tuning width. Our method has the further advantage of offering criteria for accepting or rejecting data from different regions of a mapped area. A suitable threshold can be chosen and, if the goodness of fit exceeds it, the data point in question can be excluded from subsequent analysis. If the fitting process does not converge, or returns parameters that are outside expected ranges it is likely that the data being analyzed are noisy or uninformative and should be excluded from subsequent analyses.

The Relationship Between Orientation and Direction Preference

Our method does not rigidly constrain orientation and direction preferences to be orthogonal but it may be biased to do so because we have defined, as is conventional, the direction of motion of the stimulus as orthogonal to its orientation. Whether or not orientation and direction preferences are orthogonal is arguably an empirical question that can only be answered by using stationary oriented stimuli to measure orientation preference, and moving dots to measure direction preference. Such data as exist suggest that these types of stimuli yield orientation and direction maps similar to those obtained with moving gratings. For example, orientation maps obtained with stationary, phase-reversing gratings are similar to those obtained with moving gratings (A. Shmuel and A. Grinvald, unpublished results). Likewise, the spatial pattern of regions responding differentially to directions of motion 180º apart is similar for moving dots, moving bars or moving grating stimuli [Fig. 5 in (Shmuel and Grinvald, 1996)].

Directional tuning curves obtained in single cell recordings in which noise patterns are used as stimuli are often bimodal with peaks symmetrically placed on either side of the direction preference for gratings (Hammond and Reck, 1980). The spacing between these peaks increases with the velocity of the stimulus. This suggests that direction and orientation preference can vary independently, are often non-orthogonal and even, for direction, non-unique. However such bimodal responses can probably be explained by spatio-temporal filtering of random noise by an oriented receptive field in which temporally specific interactions are exerted symmetrically along the cell's orientation axis (Skottun *et al.*, 1994). This symmetry would in fact guarantee orthogonal orientation and direction preferences for stationary versus moving gratings.

The Baseline Response

Measurement of orientation tuning width requires the establishment of a baseline in order that a width at half-height can be calculated. We defined the baseline as the part of the optical response that is common to all the stimuli, i.e. the minimum response taken across all the stimulus conditions for each pixel in the image. One reason for defining tuning parameters in this way is that a portion of the optical response to a stimulus is always non-specific and independent of the particular stimulus, i.e. the orientation or direction of motion (Bonhoeffer and Grinvald, 1996). This component of the optical signal, termed the 'non-mapping signal' might be caused by synaptic activity (Logothetis *et al.*, 2001), or in part by neuronal spiking activity. It may also reflect spatially non-specific hemodynamic responses (Malonek and Grinvald, 1996). However it is difficult if not impossible to separate these putative components. We suggest that the best way of dealing with this problem is to *define* the mapping signal as we have done here, in terms of the height above a common background.

Our analysis suggests that, on average, the baseline signal is larger near singularity locations than elsewhere (Figs 7 and 11). Possible reasons for this include: (i) hemodynamic and/or optical blurring, which would be expected to elevate the baseline in regions of high orientation gradient; (ii) increased broadening of tuning curve width near singularities, which may result in an artifactual elevation in the measured baseline, since if there is a response component at the orthogonal orientation it will be subtracted out by our method; (iii) sub-threshold neural responses which may be larger near singularities (Schummers *et al.*, 2001); and finally, (iv) an increase in the stimulus non-specific physiological spiking response at or near singularities. Regarding the latter, single-unit recording studies have demonstrated small responses to the non-preferred orientation in some neurons in cats (Azouz *et al.*, 1997) and monkeys (Ringach *et al.*, 2002); however, whether these responses increase near singularities is not yet known. The possible consequences for our results, if explanations (i) and (ii) are correct, are that, near singularities, tuning widths may be broader, and response heights larger, than our analysis suggests. It is important to note, however, that there is not an obvious, systematic relation between baseline height and tuning curve height and width that is clearly evident at all singularities. Thus it seems unlikely that the height and width variations that we see are distorted significantly by the subtraction of the baseline as we have defined it.

The Spatial Pattern of Orientation Tuning Width and Height

Our results show, we believe for the first time, that orientation tuning width and height vary independently across the surface of the cortex (Fig. 8). Tuning height correlates well with vector magnitude, and varies in the way previously described for it (Blasdel and Salama, 1986; Bonhoeffer and Grinvald, 1991, 1993; Blasdel, 1992). It is low in blob-shaped regions ~500 μm in diameter (Figs 4–6), nearly all of which contain an orientation singularity. Tuning width varies in a pattern that has not been reported before. It is broadest in narrow punctate or elongated regions that coincide exactly with the singularities, around which regions of narrow and wide tuning width often alternate in a spoke-like fashion (Figs 4*c*, 5*c*, 8 and 9*a*).

The finding of regions of high orientation selectivity close to singularities (i.e. within 200 μm), albeit with low response magnitudes, is consistent with single-unit studies that have reported that the selectivities of neurons close to singularities are as high as they are elsewhere (Maldonado *et al.*, 1997). Systematic variations in tuning width also occur in regions distant from the singularities. The strong correlation between width and the orientation gradient (Fig. 3*b*) suggests that blurring might be a cause of width variations, since it would be expected to broaden tuning curves most in regions where orientation gradient was largest. Control calculations confirmed that isotropic Gaussian blurring can reproduce some, although not all, of the observed variation in tuning width (Fig. 10). Blur could be caused by signals from out of focus layers and by the local averaging of neural activity that determines the hemodynamic response that ultimately gives rise to the optical signal. Local physiological interactions may also mimic blur. These interactions could be mediated by the dense network of

local (<400 μm) intracortical connections which has been shown to be unselective for orientation in the supragranular layers (Malach *et al.*, 1993; Bosking *et al.*, 1997). Assuming that feed-forward and other sources of input endowed all neurons in the map with the same initial degree of selectivity, these connections would have the effect of smoothing the tuning curves of individual neurons in much the same way as was done here in our control calculations, thereby inducing a positive correlation between tuning width and orientation gradient.

Evidence that the variations in tuning width are not completely the result of either optical or hemodynamic blurring of signals comes from tetrode recording experiments (Hetherington and Swindale, 1999) which showed a strong positive correlation between orientation tuning width and variation of orientation preference among groups of nearby neurons. This is consistent with the correlation between orientation gradient and tuning width observed here (Fig. 3*b*). Further evidence for physiological variations in tuning width across the map and around singularities comes from a study that combined intracellular recording with optical imaging of intrinsic signals (Schummers *et al.*, 2001). The orientation tuning width of membrane potentials of neurons in the vicinity of singularities was found to be wider on average than elsewhere. This suggests that the tuning width of a neuron is a function of the distribution of orientation preferences of neurons in its immediate vicinity. Since synaptic activity provides a major contribution to the hemodynamic response (Logothetis *et al.*, 2001), Schummers *et al.*'s findings suggest that the spatial variations of tuning width (Figs 4*c* and 5*c*) represent similar variations in the tuning of the underlying electrical activity.

Although control calculations show that isotropic Gaussian blurring can reproduce some of the observed variation in tuning widths, it cannot account for all of it (Fig. 10, Table 5). Thus non-isotropic or non-Gaussian local network interactions (Bosking *et al.*, 1997; Sincich and Blasdel, 2001) may need to be invoked to explain the correlation between orientation gradient and tuning width.

The Direction Fractures

A topological argument (Swindale *et al.*, 1987) shows that, given half-rotation orientation singularities and an orthogonal relationship between direction and orientation preferences, at least one or an odd number of direction fracture lines must connect with each orientation singularity. This was clearly observed in the present study. Similar direction fracture regions, bearing the same relationship to orientation singularities, have been described before (Swindale *et al.*, 1987; Malonek *et al.*, 1994; Shmuel and Grinvald, 1996; Weliky *et al.*, 1996; Kim *et al.*, 1999; Kisvardáy *et al.*, 2001). However, with the exception of the last two of these studies, which did not use vector averaging, the relationship between regions of high direction gradient and the singularities was not as clear-cut as seen here. This is almost certainly the result of deviations from orthogonality produced by the vector method, which tend to be greatest near orientation singularities and direction fractures. As a result, the direction fractures often terminate near a singularity, rather than in the singularity itself.

Direction fracture lines appear to have a tendency to equidistant spacing, and it is hard to find circular regions with a diameter larger than ~0.75 mm within which one or more fracture lines do not occur. This is true even in regions that lack orientation singularities (e.g. Fig. 5*f*). Such behaviors might be expected on the grounds of coverage uniformity (Swindale, 1991), i.e. that the cortex attempts to represent all possible directions of motion as uniformly as possible across the map, as seems to be true for other parameters (Swindale *et al.*, 2000). Having the fracture lines divide iso-orientation domains into equally sized sub-regions preferring opposite directions of motion might be one way to do this. Fractures also have a tendency to run in straight lines before suddenly changing direction. While this behavior tends to minimize their length, there must be other constraints on their arrangement. It would certainly be possible to connect the singularities (e.g. in Fig. 4*f*) by shorter routes than the ones actually present. However, such an arrangement, although it would give a more continuous direction map, might give poorer coverage. It remains to be seen whether or not the arrangement of direction fractures that we observe represents an optimal trade-off between smoothness and coverage constraints.

Notes

We thank Dahlia Sharon for her comments on the manuscript. This work was supported by grants from the Canadian Institutes of Health Research and the National Science and Engineering Research Council of Canada to N.V.S., by a grant from the Gorodetsky Center to A.G. and a European Molecular Biology Organization long-term fellowship for A.S.

Address correspondence to Dr Nicholas V. Swindale, Department of Ophthalmology, University of British Columbia, 2550 Willow St., Vancouver, BC, Canada, V5Z 3N9. Email: swindale@interchange.ubc.ca.

References

Azouz R, Gray CM, Nowak L, McCormick DA (1997) Physiological properties of inhibitory interneurons in cat striate cortex. Cereb Cortex 7:534–545.

Blasdel GG (1992) Orientation selectivity, preference, and continuity in monkey striate cortex. J Neurosci 12:3139–3161.

Blasdel GG, Salama G (1986) Voltage sensitive dyes reveal a modular organization in monkey striate cortex. Nature 321:579–585.

Bonhoeffer T, Grinvald A (1991) Orientation columns in cat are organized in pin-wheel like patterns. Nature 353:429–431.

Bonhoeffer T, Grinvald A (1993) The layout of iso-orientation domains in area 18 of cat visual cortex: optical imaging reveals a pinwheel-like organisation. J Neurosci 13:4157–4180.

Bonhoeffer T, Grinvald A (1996) Optical imaging based on intrinsic signals: the methodology. In: Brain mapping: the methods (Toga AW, Mazziotta JC, eds), pp. 55–97. San Diego: Academic Press.

Bonhoeffer T, Kim D-S, Malonek D, Shoham D, Grinvald A (1995) Optical imaging of the layout of functional domains in area 17 and across the area 17/18 border in cat visual cortex. Eur J Neurosci 7:1973–1988.

Bosking WH, Zhang Y, Schofield B, Fitzpatrick D (1997) Orientation selectivity and the arrangement of horizontal connections in tree shrew striate cortex. J Neurosci 17:2112–2127.

Hammond P, Reck J (1980) Influence of velocity on directional tuning of complex cells in cat striate cortex for texture motion. Neurosci Lett 19:309–314.

Hetherington PA, Swindale NV (1999) Receptive field and orientation scatter studied by tetrode recordings in cat area 17. Vis Neurosci 16:637–652.

Kim DS, Matsuda Y, Ohki K, Ajima A, Tanaka S (1999) Geometrical and topological relationships between multiple functional maps in cat primary visual cortex. Neuroreport 10:2515–2522.

Kisvardáy Z, Buzás P, Eysel U (2001) Calculating direction maps from intrinsic signals revealed by optical imaging. Cereb Cortex 11: 636–647.

Logothetis NK, Pauls J, Augath M, Trinath T, Oeltermann A (2001) Neurophysiological investigation of the basis of the fMRI signal. Nature 412:150–157.

Malach R, Amir Y, Harel M, Grinvald A (1993) Relationship between intrinsic connections and functional architecture revealed by optical imaging and *in vivo* targeted biocytin injections in primate striate cortex. Proc Natl Acad Sci USA 90:10469–10473.

Maldonado PE, Gödecke I, Gray CM, Bonhoeffer T (1997) Orientation selectivity in pinwheel centers in cat striate cortex. Science 276:1551–1555.

Malonek D, Grinvald A (1996) The spatial and temporal relationship between cortical electrical activity and responses of the microcirculation during sensory stimulation: implications for optical, PET, and MR functional brain imaging. Science 272:551–554.
Malonek D, Tootell RB, Grinvald A (1994) Optical imaging reveals the functional architecture of neurons processing shape and motion in owl monkey area MT. Proc R Soc Lond B 258:109–119.
Press WH, Teukolsky SA, Vetterling WT, Flannery BP (1994) Numerical recipes: the art of scientific computing, 2nd edn. Cambridge: Cambridge University Press.
Ringach DL, Shapley RM, Hawken MJ (2002) Orientation selectivity in macaque V1: diversity and laminar dependence. J Neurosci 22:5639–5651.
Schummers J, Mariño J, Sur M (2001) Synaptic integration by V1 neurons depends on location within the orientation map. Neuron 36:969–978.
Sharon D, Grinvald A (2002) Dynamics and constancy in cortical spatiotemporal patterns of orientation processing. Science, 295:512–515.
Shmuel A, Grinvald A (1996) Functional organization for direction of motion and its relationship to orientation maps in cat area 18. J Neurosci 16:6945–6964.
Shmuel A, Grinvald A (2000) Coexistence of linear zones and pinwheels within orientation maps in cat visual cortex. Proc Natl Acad Sci USA 97:5568–5573.
Sincich LC, Blasdel GG (2001) Oriented axon projections in primary visual cortex of the monkey. J Neurosci 21:4416–4426.
Skottun BC, Zhang J, Grosof DH (1994) On the directional selectivity of cells in the visual cortex to drifting dot patterns. Vis Neurosci 11:885–897.
Swindale NV (1991) Coverage and the design of striate cortex. Biol Cybern 65:415–424.
Swindale NV (1998) Orientation tuning curves: empirical description and estimation of parameters. Biol Cybern 78:45–56.
Swindale NV, Matsubara JA, Cynader MS (1987) Surface organization of orientation and direction selectivity in cat area 18. J Neurosci 7:1414–1427.
Swindale NV, Shoham D, Grinvald A, Bonhoeffer T, Hübener M (2000) Visual cortex maps are optimized for uniform coverage. Nat Neurosci 3:822–826.
Weliky M, Bosking WH, Fitzpatrick DA (1996) Systematic map of direction preference in primary visual cortex. Nature 379:725–728.
Wörgötter F, Eysel U Th (1987) Quantitative determination of orientational and directional components in the response of visual cortical cells to moving stimuli. Biol Cybern 57:349–355.